Journal of Computational Electronics (2018) 17:909–919
https://doi.org/10.1007/s10825-018-1192-y

Theoretical investigation of electronic performance, half-metallicity, and magnetic properties of Cr-substituted BaTe

Khelifa Berriah[1] · Bendouma Doumi[2] · Allel Mokaddem[3,4] · Mohammed Elkeurti[1,2] · Adlane Sayede[5] · Abdelkader Tadjer[6] · João Pedro Araújo[7]

Published online: 2 June 2018

Abstract
We have investigated the structural, electronic, and ferromagnetic properties of chromium (Cr)-doped rocksalt BaTe ($Ba_{1-x}Cr_xTe$) compounds with compositions $x = 0.25$, 0.5, and 0.75, based on density functional theory with generalized gradient approximation of Wu–Cohen (GGA-WC) and Tran–Blaha-modified Becke–Johnson (TB-mBJ) potential using the WIEN2k package. We found that the electronic structure showed half-metallic ferromagnetic character with spin polarization of 100 % around the Fermi level. In addition, the minority-spin bands depicted a half-metallic ferromagnetic (HMF) gap and half-metallic (HM) gap. The improved HMF and HM gaps found with the TB-mBJ potential are higher than with the GGA-WC approximation. These large HM gaps make $Ba_{1-x}Cr_xTe$ compounds promising candidates for use in spintronics applications.

Keywords Cr-substituted BaTe · TB-mBJ approach · Half-metallic ferromagnetism · Electronic properties

1 Introduction

In recent years, a new field of electronics called spintronics has been developing rapidly [1–3]. In this approach, the electron spin is used as another degree of freedom for information processing, offering a promising method to meet new challenges [2,4]. Spintronics devices offer several advantages compared with conventional electronics, including higher speed and lower power, because they are based on spin direction and spin coupling [5]. In particular, transition-metal-doped III–V and II–VI semiconductors have emerged as a new type of compounds called dilute magnetic semiconductors (DMSs). These materials are main candidates for progress of spintronics applications, because they are ferromagnetically stable at higher temperatures than room temperature [6,7] and exhibit half-metallic ferromagnetic behavior [8–10].

The BaX (X = S, Se, Te) barium chalcogenides belong to the group of alkaline-earth chalcogenides, which are wide-gap insulators with closed-shell ionic systems [11]. BaX compounds have attracted increasing attention because of their potential applications in light-emitting and laser diodes [12–14] as well as luminescent and magnetooptical devices [15–18]. BaTe forms closed-shell ionic coordination and crystallizes as an NaCl-type (B1) phase at ambient conditions

✉ Khelifa Berriah
khelifaberiah@gmail.com

✉ Bendouma Doumi
bdoummi@yahoo.fr

✉ Allel Mokaddem
mokaddem.allel@gmail.com

1 Laboratory of Physico-Chemical Studies, University of Saida, 20000 Saida, Algeria

2 Department of Physics, Faculty of Sciences, Dr. Tahar Moulay University of Saida, 20000 Saida, Algeria

3 Centre Universitaire Nour Bachir El Bayadh, 32000 El Bayadh, Algeria

4 Theoretical Physics Laboratory, U.S.T.H.B., Algiers, Algeria

5 Unité de Catalyse et Chimie du Solide (UCCS), UMR CNRS 8181, Faculté des Sciences, Université d'Artois, Rue Jean Souvraz, SP 18, 62307 Lens, France

6 Modelling and Simulation in Materials Science Laboratory, Physics Department, Djillali Liabes University of Sidi Bel-Abbes, 22000 Sidi Bel-Abbes, Algeria

7 IFIMUP and IN-Institute of Nanoscience and Nanotechnology, Universidade do Porto, 4169-007 Porto, Portugal

[14,19]; it has been widely researched owing to its interesting structural and electronic properties [14]. Syassen et al. [20] found that optical and absorption spectra of BaTe appear in the pressure range of 0–400 kPa at temperature of 300 K. Besides, Feng et al. [14] investigated the effect of spin–orbit coupling on the optical properties of BaTe, including the reflectivity and the real and imaginary parts of the dielectric function. BaTe has an indirect gap located between the Γ and X high-symmetry points, exhibiting a reduction of about 0.27 eV in its bandgap on application of spin–orbit coupling [21].

Recently, several experimental and theoretical works have been carried out on the half-metallic and magnetic properties of DMSs based on II–VI semiconductors, e.g., on the room-temperature ferromagnetism of half-metallic Ni-doped ZnS [22], half-metallic ferromagnetism of Fe-doped ZnS thin films formed by chemical bath deposition [23], half-metallic ferromagnetism of Co- and Fe-doped CdSe [24], half-metallic ferromagnetism in V-doped ZnS [25], and half-metallic ferromagnetic properties of V-doped BaS [26] and V-doped SrO [27].

To the best of the authors' knowledge, no experimental and theoretical studies have been performed on BaTe doped with chromium (Cr) atom. In the work presented herein, we investigated the half-metallic ferromagnetic behavior and improved electronic structure of Cr-doped BaTe to explore its ferromagnetic features for use in spintronic applications. For these calculations, we used first-principles calculations based on density functional theory (DFT) using the WIEN2k code [28] [29,30], treating the exchange and correlation potential using the Wu–Cohen generalized gradient approximation (GGA-WC) [31] and Tran–Blaha-modified Becke–Johnson (TB-mBJ) approach [32,33].

2 Calculation methods

We employed the WIEN2k package [28] based on the full-potential linearized augmented plane-wave (FP-LAPW) method for first-principles DFT calculations [29,30] to study the structural, electronic, and magnetic properties of $Ba_{1-x}Cr_xTe$ compounds with various compositions $x = 0.25$, 0.5, and 0.75 of chromium (Cr) impurity. First, we calculated the structural parameters, electronic structure, and magnetic properties, using the Wu–Cohen generalized gradient approximation (GGA-WC) [31]. We then used the accurate Tran–Blaha-modified Becke–Johnson (TB-mBJ) exchange potential combined with the local density correlation potential [32,33] to improve the electronic properties and give the exact gaps of the band structure.

We chose the average of the muffin-tin radii of Ba, Te, and Cr atoms in such a way that the muffin-tin spheres do not overlap. Besides, the charge density was Fourier extended up to $G_{max} = 14$ (a.u.)$^{-1}$, where G_{max} is the largest vector of the Fourier expansion. We extended the basis functions and potential in combination with spherical harmonics around atomic sites with cutoff of $l_{max} = 10$. In the interstitial region, the Fourier series were extended in plane waves with cutoff of R_{MT} $K_{max} = 9$ (where R_{MT} is the mean radius of the muffin-tin spheres). For Brillouin zone sampling, we utilized a Monkhorst–Pack mesh [34,35] of $(4 \times 4 \times 4)$ for BaTe, $Ba_{0.75}Cr_{0.25}Te$, and $Ba_{0.25}Cr_{0.75}Te$, and $(4 \times 4 \times 3)$ for $Ba_{0.5}Cr_{0.5}Te$, with self-consistent convergence of the total energy of 0.1 mRy. Note that the number of **k**-points was reduced in the tetragonal structure of $Ba_{0.5}Cr_{0.5}Te$ in space group $P4/mmm$ (no. 123) due to its lower number of symmetry operations compared with the cubic structure of $Ba_{0.75}Cr_{0.25}Te$ and $Ba_{0.25}Cr_{0.75}Te$ in space group $Pm\bar{3}m$ (no. 221).

3 Results and discussion

3.1 Structural parameters

Barium telluride (BaTe) crystallizes in a rocksalt NaCl (B1) phase; its conventional structure has two types of atoms, viz. Ba and Te, located at (0, 0, 0) and (0.5, 0.5, 0.5) positions, respectively, with space group $Fm\bar{3}m$ (no. 225). In the Ba_4Te_4 structure with eight atoms, we substituted one, two, or three atoms of chromium (Cr) at Ba sites to create supercells of $Ba_{0.75}Cr_{0.25}Te$, $Ba_{0.5}Cr_{0.5}Te$, and $Ba_{0.25}Cr_{0.75}Te$ with concentration $x = 0.25$, 0.5, and 0.75, respectively. The $Ba_{0.75}Cr_{0.25}Te$ and $Ba_{0.25}Cr_{0.75}Te$ supercells have cubic structure in space group $Pm\bar{3}m$ (no. 221), while $Ba_{0.5}Cr_{0.5}Te$ has tetragonal structure in space group $P4/mmm$ (no. 123). Note that the description of the $Ba_{0.75}Cr_{0.25}Te$, $Ba_{0.5}Cr_{0.5}Te$, and $Ba_{0.25}Cr_{0.75}Te$ alloys using smaller supercells would necessarily introduce side effects on their ordered structure. Therefore, our calculations are valid only for ordered structures close to the stoichiometries of the ordered $Ba_{0.75}Cr_{0.25}Te$, $Ba_{0.5}Cr_{0.5}Te$, and $Ba_{0.25}Cr_{0.75}Te$ compounds.

Structural parameters of BaTe and $Ba_{1-x}Cr_xTe$ at various concentrations were determined by fitting the variation of the total energy as a function of volume using the Murnaghan equation [36]. The structural parameters such as the lattice constant (a), bulk modulus (B), and its pressure derivative (B') calculated for BaTe and $Ba_{1-x}Cr_xTe$ at different concentrations using the GGA-WC approximation, together with other theoretical [37–40] and experimental data [41], are summarized in Table 1. The a and B parameters obtained for BaTe are in good agreement with experimental [41] and recent theoretical calculations [37,38] using the GGA-WC approximation [31]. In addition, the

Table 1 Calculated lattice constant (a), bulk modulus (B), and its pressure derivative (B') for BaTe and $Ba_{1-x}Cr_xTe$ with composition $x = 0.25$, 0.5, and 0.75 of Cr atoms

Compound	a (Å)	B (GPa)	B'	Method
This work				GGA-WC
BaTe	6.944	31.89	4.56	
$Ba_{0.75}Cr_{0.25}Te$	6.735	33.51	5.02	
$Ba_{0.5}Cr_{0.5}Te$	6.457	38.27	5.47	
$Ba_{0.25}Cr_{0.75}Te$	6.073	50.66	6.42	
Other calculations				
BaTe	6.934 [37]	28.81 [37]	5.191 [37]	GGA-WC
	6.955 [38]	30.91 [38]	4.012 [38]	GGA-WC
	7.075 [39]	27.04 [39]	4.63 [39]	GGA-PBE
	7.0667 [40]	28.5384 [40]	4.0526 [40]	GGA-PBE
	6.8690 [40]	35.3052 [40]	4.4247 [40]	LDA
	7.005 [41]	29.4 [41]	7.4 [41]	Experimental

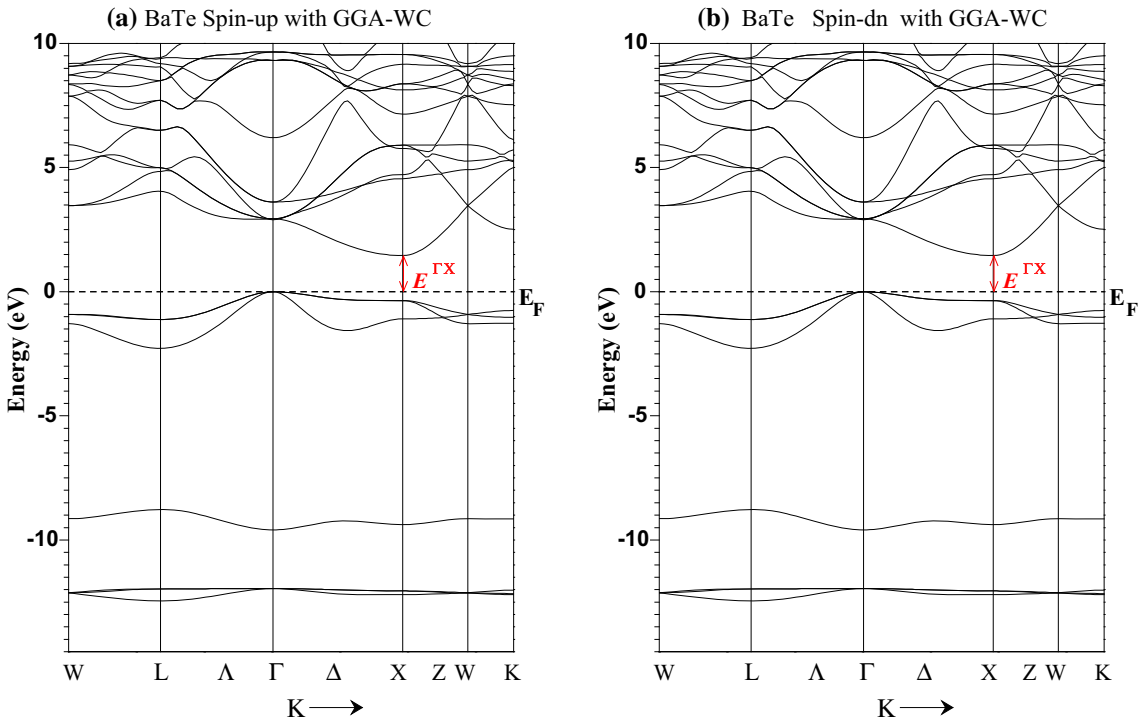

Fig. 1 Spin-polarized band structure obtained with GGA-WC for BaTe: **a** majority spin (up) and **b** minority spin (dn). The Fermi level is set to zero (horizontal dotted line)

results of these parameters are better than recent calculations [39,40] using the generalized gradient approximation of Perdew–Burke–Ernzerhof (GGA-PBE) [42] and local density approximation (LDA) with Teter–Pade parameterization [43]. This is due to the precise GGA-WC exchange potential for structural properties. For the doped $Ba_{1-x}Cr_xTe$ system, the lattice constant decreased with increasing concentration of chromium owing to the difference between the ionic radii of the Ba atom and the substituted Cr impurity. Consequently, $Ba_{1-x}Cr_xTe$ becomes harder with increasing Cr concentration. Note that there are no experimental and theoretical calculations to compare with our results for the structural parameters of $Ba_{0.75}Cr_{0.25}Te$, $Ba_{0.5}Cr_{0.5}Te$, and $Ba_{0.25}Cr_{0.75}Te$.

3.2 Electronic structure and half-metallic performance

We calculated the spin-polarized densities of states (DOS) and band structures of the BaTe and $Ba_{1-x}Cr_xTe$ materials using the optimized lattice constants. Firstly, we used the GGA-WC approximation to calculate the electronic structure

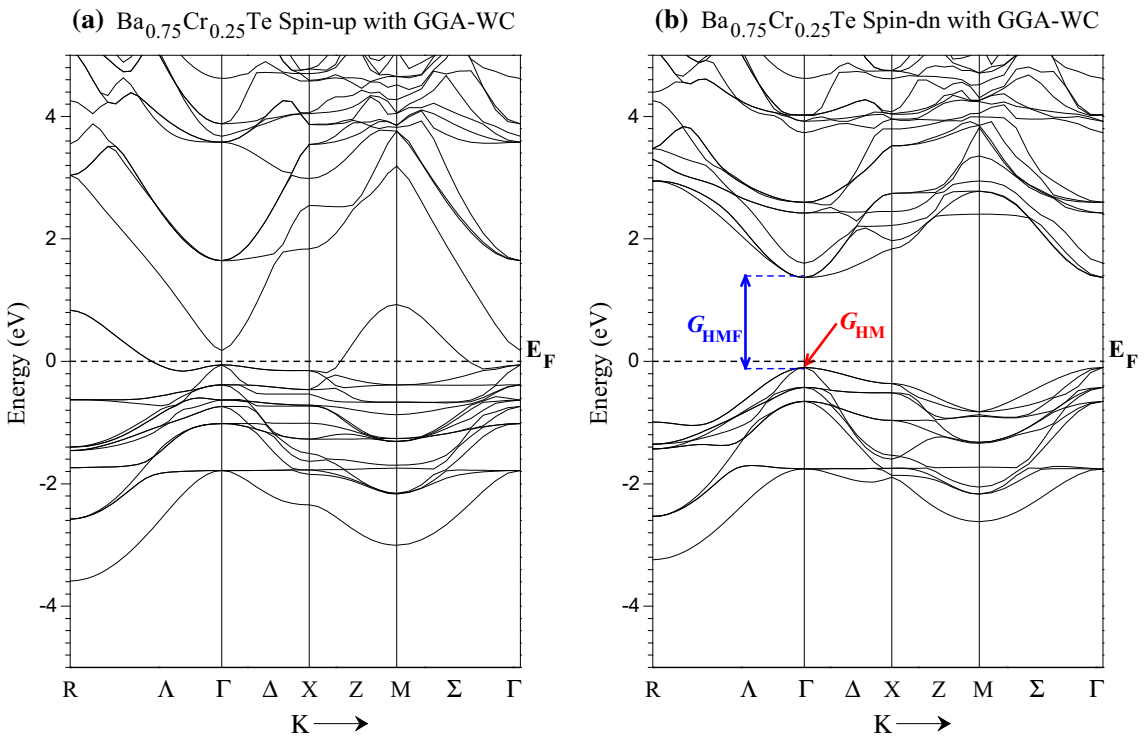

Fig. 2 Spin-polarized band structure obtained with GGA-WC for $Ba_{0.75}Cr_{0.25}Te$: **a** majority spin (up) and **b** minority spin (dn). The Fermi level is set to zero (horizontal dotted line)

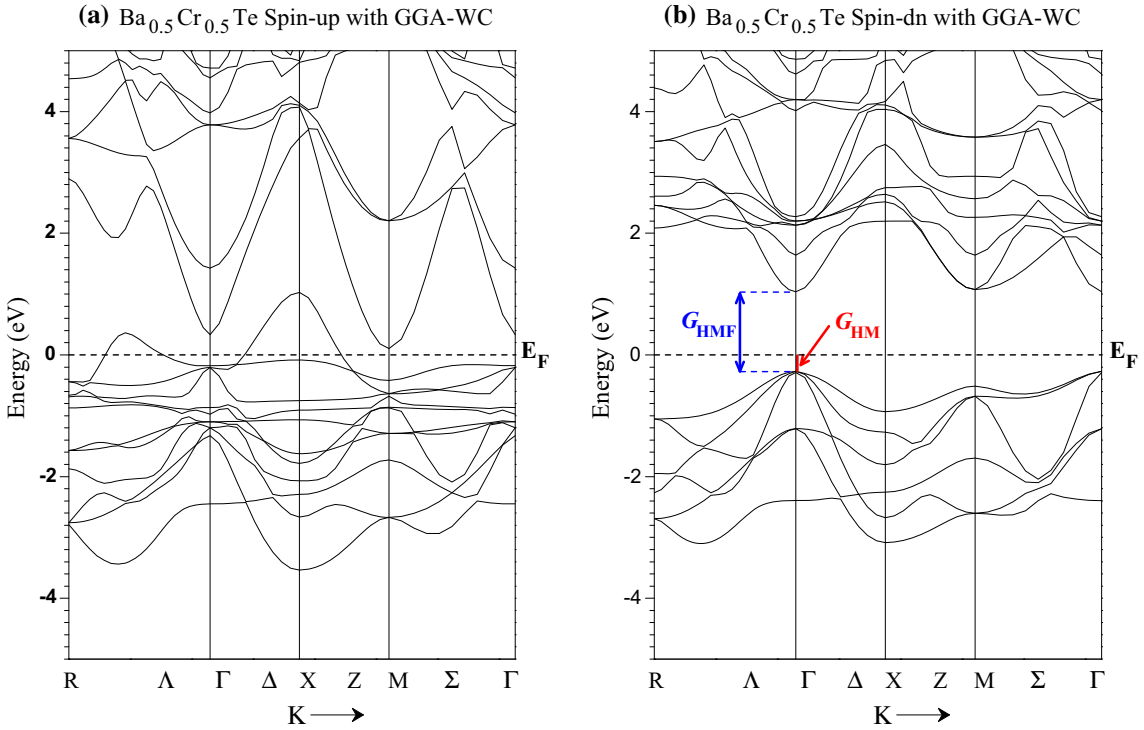

Fig. 3 Spin-polarized band structure obtained with GGA-WC for $Ba_{0.5}Cr_{0.5}Te$: **a** majority spin (up) and **b** minority spin (dn). The Fermi level is set to zero (horizontal dotted line)

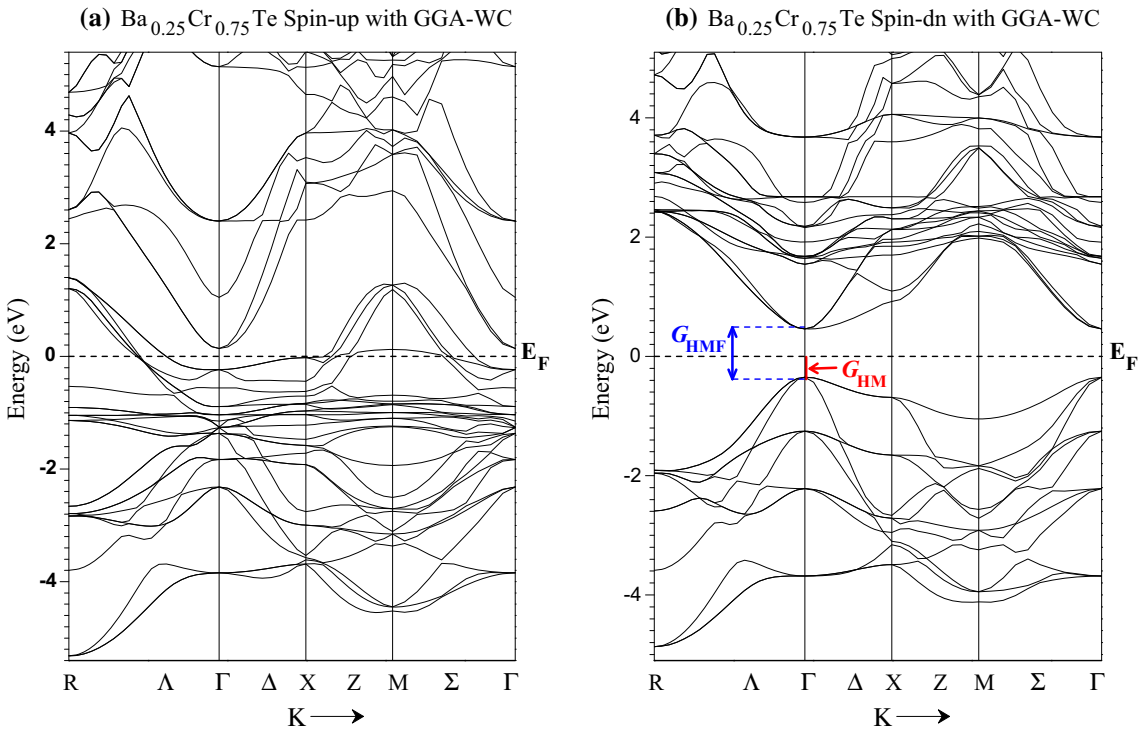

Fig. 4 Spin-polarized band structure obtained with GGA-WC for $Ba_{0.25}Cr_{0.75}Te$: **a** majority spin (up) and **b** minority spin (dn). The Fermi level is set to zero (horizontal dotted line)

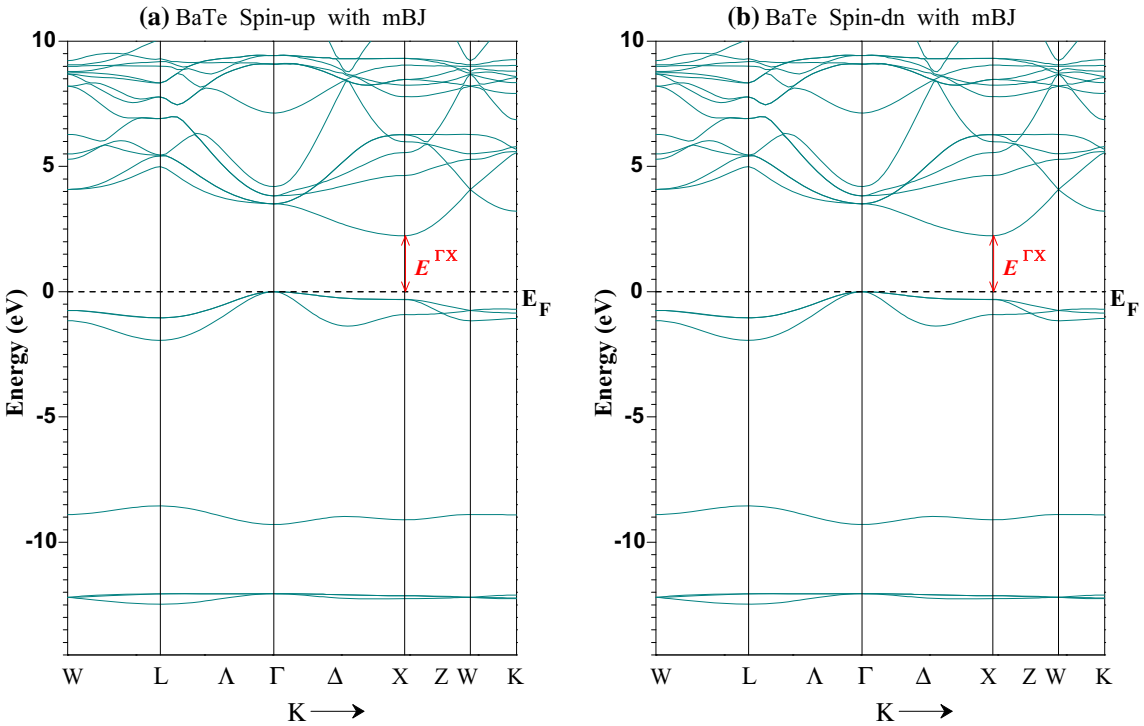

Fig. 5 Spin-polarized band structure obtained with TB-mBJ for BaTe: **a** majority spin (up) and **b** minority spin (dn). The Fermi level is set to zero (horizontal dotted line)

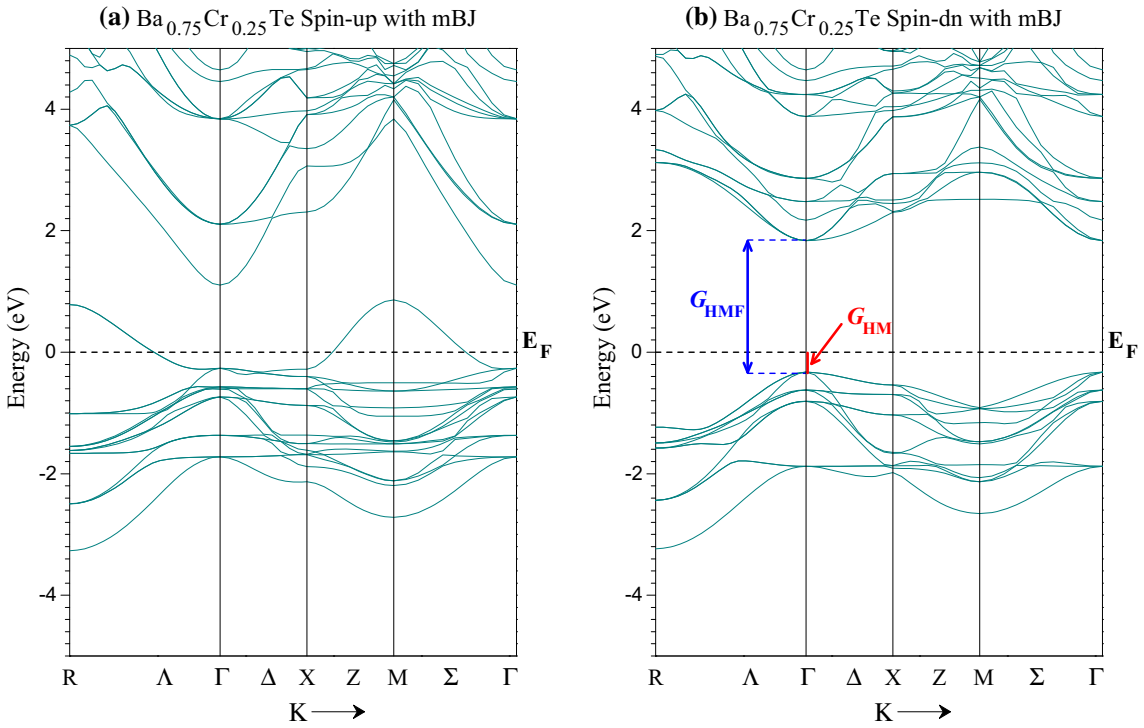

Fig. 6 Spin-polarized band structure obtained with TB-mBJ for $Ba_{0.75}Cr_{0.25}Te$: **a** majority spin (up) and **b** minority spin (dn). The Fermi level is set to zero (horizontal dotted line)

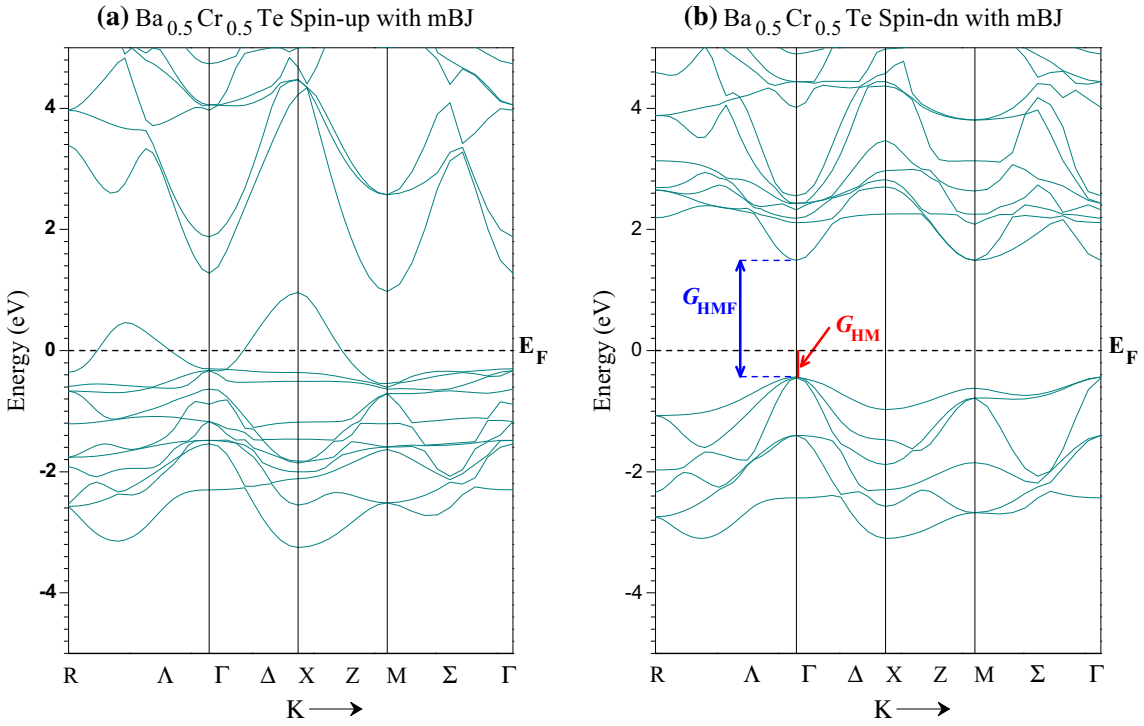

Fig. 7 Spin-polarized band structure obtained with TB-mBJ for $Ba_{0.5}Cr_{0.5}Te$: **a** majority spin (up) and **b** minority spin (dn). The Fermi level is set to zero (horizontal dotted line)

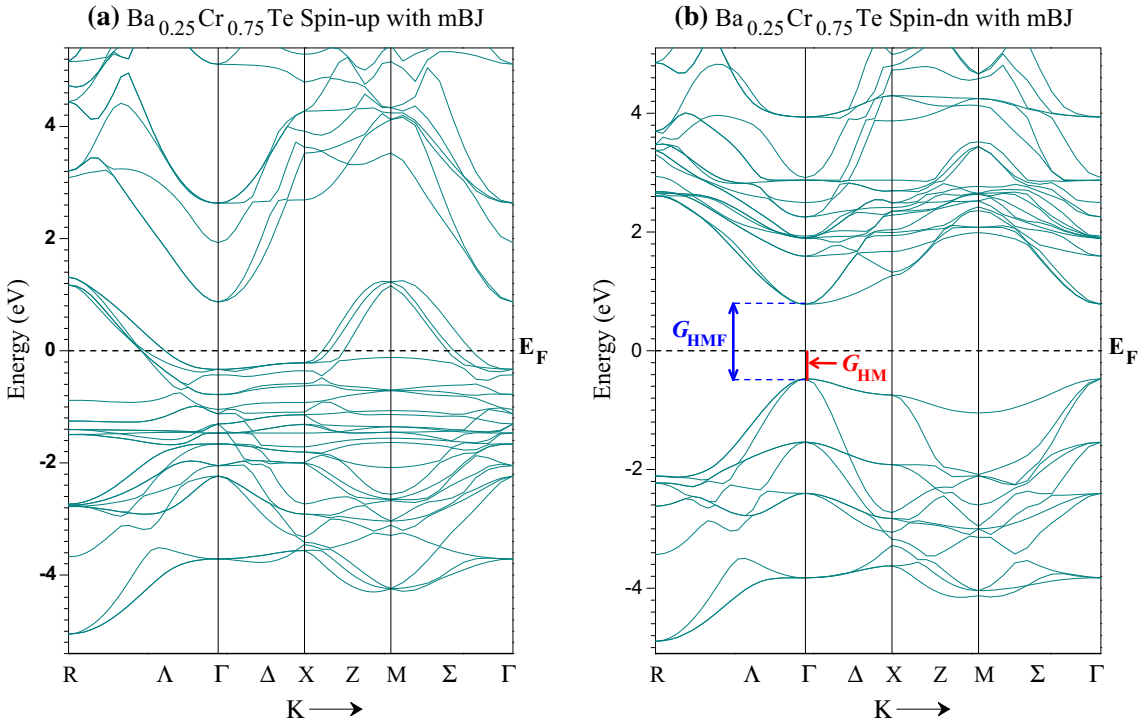

Fig. 8 Spin-polarized band structure obtained with TB-mBJ for $Ba_{0.25}Cr_{0.75}Te$: **a** majority spin (up) and **b** minority spin (dn). The Fermi level is set to zero (horizontal dotted line)

Table 2 Calculated indirect bandgap ($E^{\Gamma}X$) for BaTe, half-metallic ferromagnetic gap (G_{HMF}), and half-metallic gap (G_{HM}) of minority-spin bands for $Ba_{1-x}Cr_xTe$ at concentrations $x = 0.25$, 0.5, and 0.75 of Cr atoms

Compound	G_{HMF}(eV)	G_{HM}(eV)	$E^{\Gamma}X$ (eV)	Method	Behavior
This work				GGA-WC	
BaTe			1.455		
$Ba_{0.75}Cr_{0.25}Te$	1.491	0.136			HMF
$Ba_{0.5}Cr_{0.5}Te$	1.298	0.282			HMF
$Ba_{0.25}Cr_{0.75}Te$	0.816	0.360			HMF
This work				TB-mBJ	
BaTe			2.256		
$Ba_{0.75}Cr_{0.25}Te$	2.167	0.329			HMF
$Ba_{0.5}Cr_{0.5}Te$	1.923	0.435			HMF
$Ba_{0.25}Cr_{0.75}Te$	1.250	0.469			HMF
Other calculations					
BaTe			1.325 [37], 1.822 [38]	GGA-WC	
			1.656 [39], 1.6516 [40]	GGA-PBE	
			1.3649 [40]	LDA	
			2.453 [37], 2.254 [38]	TB-mBJ	
			2.365 [39]		
			3.08 [48], 3.1 [49]	Experimental	

of the compounds. We then improved the bandgap calculations of the electronic structure using the TB-mBJ approach. The spin-polarized band structure of the compounds is shown in Figs. 1, 2, 3, and 4 for the GGA-WC and Figs. 5, 6, 7, and 8 with the TB-mBJ potential. Figures 1 and 5 show that the two spin channels of BaTe have similar semiconducting band structures with indirect bandgap ($E^{\Gamma}X$) located between Γ and X high-symmetry points. The remaining figures for $Ba_{1-x}Cr_xTe$ with each concentration reveal a half-metallic feature resulting from the metallic nature of the majority spin and a bandgap for the minority spin. The minority-spin bands of $Ba_{1-x}Cr_xTe$ reveal two types of bandgap, viz.

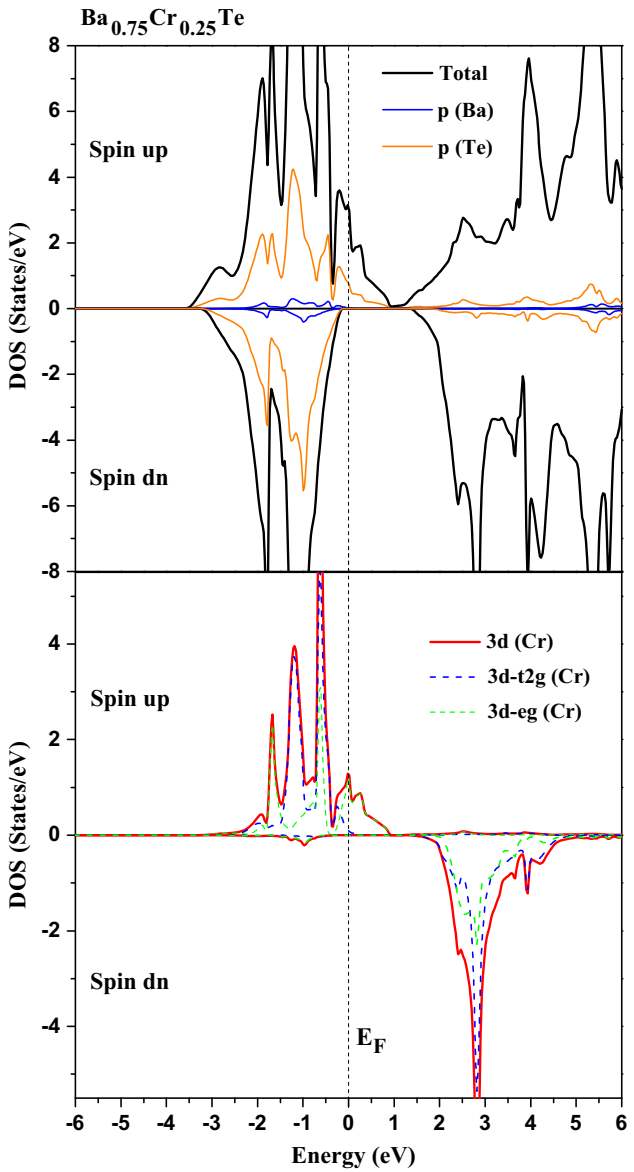

Fig. 9 Spin-polarized total and partial densities of states of $Ba_{0.75}Cr_{0.25}Te$. The Fermi level is set to zero (vertical dotted line)

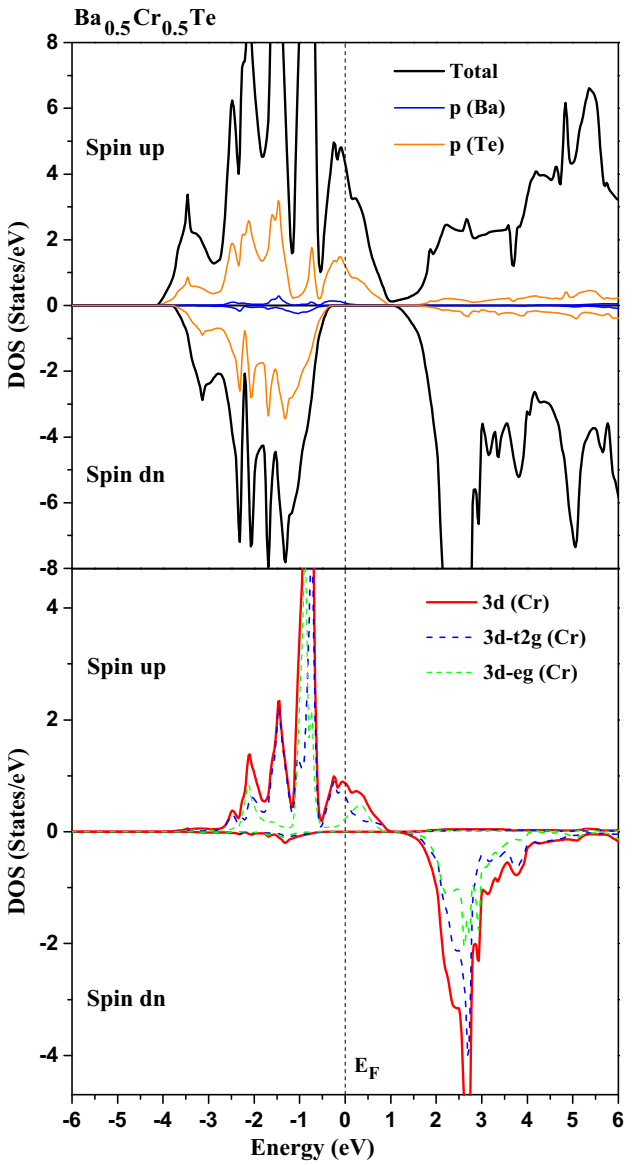

Fig. 10 Spin-polarized total and partial densities of states of $Ba_{0.5}Cr_{0.5}Te$. The Fermi level is set to zero (vertical dotted line)

a direct half-metallic ferromagnetic (HMF) gap and half-metallic (HM) gap. The direct HMF gap is situated at Γ high-symmetry point between the valence-band maximum (VBM) and conduction-band minimum (CBM). The HM gap is defined as the minimum of the lowest energy of the majority (minority)-spin conduction bands with respect to the Fermi level and the absolute value of the highest energy of the majority (minority)-spin valence bands [44,45]. This factor describes the minimal energy bandgap for a spin-flip excitation needed to create a hole or electron with minority spin [9,46,47].

The calculated indirect gap ($E^{\Gamma X}$) of BaTe, HMF (G_{HMF}) and HM (G_{HM}) gaps of $Ba_{1-x}Cr_xTe$ at all concentrations, using the GGA-WC and TB-mBJ exchange potentials, together with other theoretical [37–40] and experimental [48,49] data, are presented in Table 2. The agreement is very good between our computed $E^{\Gamma X}$ for BaTe and calculations [37,38] using the same GGA-WC and TB-mBJ approaches. Also, our result for $E^{\Gamma X}$ with TB-mBJ is better than other calculations [39,40] using the GGA-PBE [42] and LDA [43] approximations. Note that the calculated $E^{\Gamma X}$, G_{HMF}, and G_{HM} gaps obtained with TB-mBJ are higher than obtained with the GGA-WC, because the TB-mBJ semilocal exchange correlation potential can provide perfect bandgaps compared with the LDA and different versions of the GGA approxima-

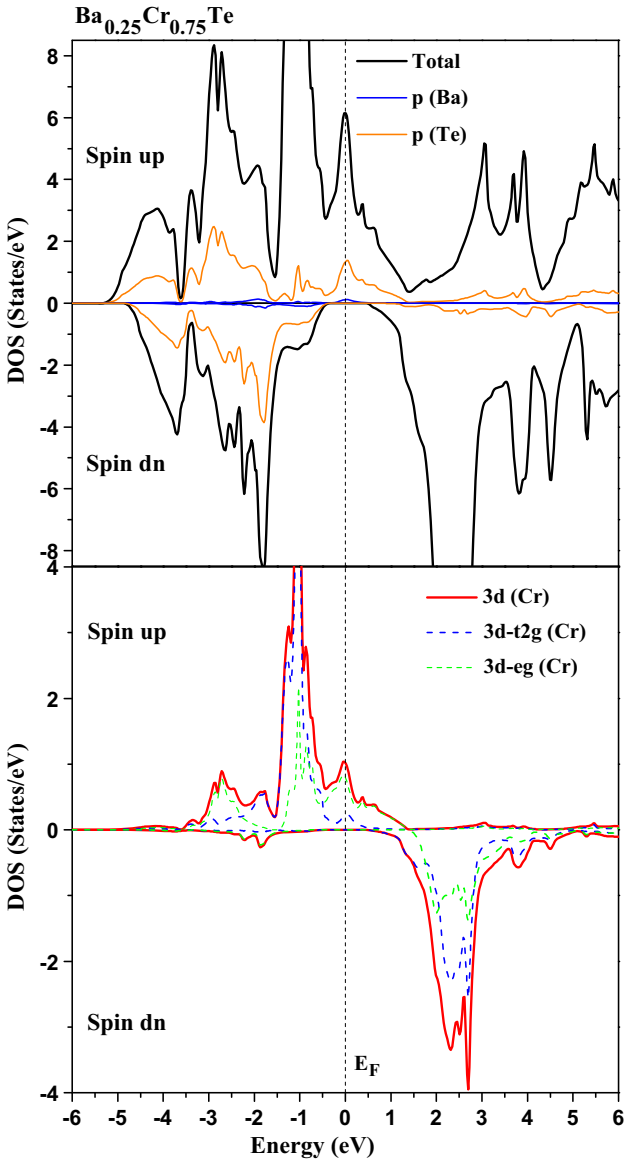

Fig. 11 Spin-polarized total and partial densities of states of $Ba_{0.25}Cr_{0.75}Te$. The Fermi level is set to zero (vertical dotted line)

tion for semiconductors and insulators [33,37,38]. Moreover, we understand that the half-metallic ferromagnetic gap of $Ba_{1-x}Cr_xTe$ decreases with increasing chromium concentration, due to broadening of 3*d* states of the Cr impurity in the gap. We found that $Ba_{0.75}Cr_{0.25}Te$, $Ba_{0.5}Cr_{0.5}Te$, and $Ba_{0.25}Cr_{0.75}Te$ compounds exhibited half-metallic character with HM gap of 0.329, 0.435, and 0.469 eV, making them promising materials for use in spintronics applications.

The contribution to the DOS around the Fermi level (E_F) determines the metallic or semiconductor nature of a material and its polarization. The spin polarization (P) of a material arises from the difference in the contribution of the densities of states of the majority spin $N^{\uparrow}(E_F)$ and minority spin

Table 3 Calculated total and local magnetic moments of relevant Cr, Ba, and Te atoms, and at interstitial sites (in Bohr magneton μ_B per Cr atom) for $Ba_{1-x}Cr_xTe$ with compositions $x = 0.25$, 0.5, and 0.75 of Cr atoms

Compound	Total (μ_B)	Cr (μ_B)	Ba (μ_B)	Te (μ_B)	Interstitial (μ_B)
This work					
$Ba_{0.75}Cr_{0.25}Te$	4	3.996	0.001	−0.261	0.265
$Ba_{0.5}Cr_{0.5}Te$	4	3.952	0.0005	−0.242	0.290
$Ba_{0.25}Cr_{0.75}Te$	4	3.788	−0.006	−0.189	0.408

$N^{\downarrow}(E_F)$ around E_F, defined by the expression [50]

$$P = \frac{N^{\uparrow}(E_F) - N^{\downarrow}(E_F)}{N^{\uparrow}(E_F) + N^{\downarrow}(E_F)}. \quad (1)$$

The spin-polarized total (T) and partial (P) densities of states (DOS) of $Ba_{0.75}Cr_{0.25}Te$, $Ba_{0.5}Cr_{0.5}Te$, and $Ba_{0.25}Cr_{0.75}Te$ compounds are shown in Figs. 9, 10, and 11, respectively. These plots depict that the valence bands of the two spin directions are dominated by the major contribution of *p* (Te) and 3*d* (Cr) states and minor *p* (Ba) states in the energy ranges of −2.5 to −0.1 eV for $Ba_{0.75}Cr_{0.25}Te$, −2.7 to −0.6 eV for $Ba_{0.5}Cr_{0.5}Te$, and −3.5 to −0.3 eV for $Ba_{0.25}Cr_{0.75}Te$. The crystal field of the octahedral (Te) surrounding splits the 3*d* (Cr) levels into two types of states, viz. three low-lying t_{2g} (d_{xy}, d_{xz}, and d_{yz}) levels and two high-lying e_g (d_{z^2} and $d_{x^2-y^2}$) states [9,46], as shown in Fig. 9. For $Ba_{1-x}Cr_xTe$ at all concentrations, the metallic nature of the majority spin results from *p–d* hybridization between *p* (Te) and 3*d* (Cr) states around E_F, while the minority-spin states show a gap. Consequently, the $Ba_{1-x}Cr_xTe$ compounds exhibit half-metallic ferromagnetic behavior with spin polarization of 100 %, making them potential candidates for use in spintronics applications.

3.3 Magnetic properties

The ferromagnetic state of $Ba_{1-x}Cr_xTe$ can be explained using the Zener carrier-mediated model [51], because the ferromagnetism is mediated by acceptor hole carriers generated by partially filled 3d (Cr) levels. Besides, the partially occupied 3*d* (Cr) states stabilize the ferromagnetic state configuration [52,53] associated with the double-exchange mechanism [54]. Therefore, the ferromagnetic state arrangement of $Ba_{1-x}Cr_xTe$ is stabilized by the contributions of *p–d* exchange and double-exchange mechanisms.

To describe the effect of the *p–d* exchange mechanism on the magnetic behavior, we calculated the total magnetic moment per Cr atom and local magnetic moments

within the muffin-tin spheres of the relevant Cr, Ba, and Te atoms in $Ba_{1-x}Cr_xTe$ compounds. The total and local magnetic moments of $Ba_{0.75}Cr_{0.25}Te$, $Ba_{0.5}Cr_{0.5}Te$, and $Ba_{0.25}Cr_{0.75}Te$ are presented in Table 3, revealing that the total magnetic moment per Cr atom for each compound was equal to $4\mu_B$, principally due to the local magnetic moment of Cr atom. The total magnetic moment of $4\mu_B$ originates from the 3*d* (Cr) majority-spin states, which are partially filled with four electrons. On the other hand, the predicted magnetic moment of Cr atom is reduced to below $4\mu_B$ and minor local magnetic moments are induced at Ba, Te, and interstitial sites due to the *p–d* exchange interaction between *p* (Te) and 3*d* (Cr) levels. For $Ba_{1-x}Cr_xTe$ at all concentrations, the magnetic spins of Cr and Te atoms have opposite sign, indicating antiferromagnetic interaction between Cr and Te. The interaction between Cr and Ba atoms is ferromagnetic for $Ba_{0.75}Cr_{0.25}Te$ and $Ba_{0.5}Cr_{0.5}Te$, but becomes antiferromagnetic in the case of $Ba_{0.25}Cr_{0.75}Te$ compound.

4 Conclusions

We predicted the structural, electronic, and ferromagnetic properties of rocksalt BaTe doped with Cr atoms, i.e., $Ba_{1-x}Cr_xTe$ with compositions $x = 0.25$, 0.5, and 0.75, based on first-principles calculations in DFT with the GGA-WC and TB-mBJ exchange potentials using WIEN2k code. The electronic structure showed that the $Ba_{1-x}Cr_xTe$ compounds are half-metallic ferromagnetic with spin polarization of 100 %. The total magnetic moment per Cr atom has integral value of $4\mu_B$, being principally formed by the main contribution of the local magnetic moment of Cr atom. The ferromagnetic state arrangement is stabilized by both *p–d* exchange and double-exchange mechanisms. The improved HM gaps of the $Ba_{1-x}Cr_xTe$ materials make them potential candidates for use in future spintronics applications.

References

1. Matsukura, F., Tokura, Y., Ohno, H.: Control of magnetism by electric fields. Nat. Nanotechnol. **10**, 209–220 (2015)
2. Nie, T., Tang, J., Wang, K.L.: Quest for high-Curie temperature Mn_xGe_{1-x} diluted magnetic semiconductors for room-temperature spintronics applications. J. Cryst. Growth **425**, 279–282 (2015)
3. Tang, J., Nie, T., Wang, K.L.: Spin transport in Ge nanowires for diluted magnetic semiconductor-based nonvolatile transpinor. ECS Trans. **64**(6), 613–623 (2014)
4. Wang, K.L., Zhao, Z., Khitun, A.: Spintronics for nanoelectronics and nanosystems. Thin Solid Films **517**, 184–190 (2008)
5. Yu, Y.B., Thompson, S.M.: Spintronic Materials and Technology. Taylor & Francis, Boca Raton (2007)
6. Sato, K., Katayama-Yoshida, H.: Material design of GaN-based ferromagnetic diluted magnetic semiconductors. Jpn. J. Appl. Phys. **40**, L485–L487 (2001)
7. Wu, S.Y., Liu, H.X., Gu, L., Singh, R.K., Budd, L., van Schilfgaarde, M., McCartney, M.R., Smith, D.J., Newman, N.: Synthesis, characterization, and modeling of high quality ferromagnetic Cr-doped AlN thin films. Appl. Phys. Lett. **82**, 3047 (2003)
8. Doumi, B., Tadjer, A., Dahmane, F., Mesri, D., Aourag, H.: Investigations of structural, electronic, and half-metallic ferromagnetic properties in $(Al,Ga,In)_{1-x}M_xN$ (M = Fe, Mn) diluted magnetic semiconductors. J. Supercond. Nov. Magn. **26**, 515 (2013)
9. Doumi, B., Mokaddem, A., Temimi, L., Beldjoudi, N., Elkeurti, M., Dahmane, F., Sayede, A., Tadjer, A., Ishak-Boushaki, M.: First-principle investigation of half-metallic ferromagnetism in octahedrally bonded Cr-doped rock-salt SrS, SrSe, and SrTe. Eur. Phys. J. B **88**, 93 (2015)
10. Berber, M., Doumi, B., Mokaddem, A., Mogulkoc, Y., Sayede, A., Tadjer, A.: Investigation of electronic structure and half-metallic ferromagnetic behavior with large half-metallic gap in $Sr_{1-x}V_xO$. J. Comput. Electron. **16**, 542–547 (2017)
11. Bhardwaj, P., Singh, S.: Pressure induced structural phase transitions—A review. Cent. Eur. J. Chem. **10**(5), 1391–1422 (2012)
12. Heng, K.L., Chua, S.J., Wu, P.: Prediction of semiconductor material properties by the properties of their constituent chemical elements. Chem. Mater. **12**, 1648–1653 (2000)
13. Tuncel, E., Colakoglu, K., Deligoz, E., Ciftci, Y.O.: A first-principles study on the structural, elastic, vibrational, and thermodynamical properties of BaX (X = S, Se, and Te). J. Phys. Chem. Solids **70**, 371–378 (2009)
14. Feng, Z., Hu, H., Lv, Z., Cui, S.: First-principles study of electronic and optical properties of BaS, BaSe and BaTe. Cent. Eur. J. Phys. **8**(5), 782–788 (2010)
15. Partin, D.L., Thrush, C.M., Clemens, B.M.: Lead strontium telluride and lead barium telluride grown by molecular-beam epitaxy. J. Vac. Sci. Technol., B **5**, 686–689 (1987)
16. Weir, S.T., Vohra, Y.K., Ruoff, A.L.: Pressure-induced metallization of BaSe. Phys. Rev. B **35**, 874 (1987)
17. Pandey, R., Sivaraman, S.: Spectroscopic properties of defects in alkaline-earth sulfides. J. Phys. Chem. Solids **52**(1), 211–225 (1991)
18. Lin, G.Q., Gong, H., Wu, P.: Electronic properties of barium chalcogenides from first-principles calculations: Tailoring wide-band-gap II–VI semiconductors. Phys. Rev. B **71**, 085203 (2005)
19. Kholiya, K., Verma, S.: Pressure-induced phase transition and elastic properties of barium chalcogenides. Phase Transit. **84**, 67–76 (2011)
20. Syassen, K., Christensen, N.E., Winzen, H.: Optical response and band-structure calculations of alkaline-earth tellurides under pressure. Phys. Rev. B **35**, 4052 (1987)
21. Pourghazi, A., Dadsetani, M.: Electronic and optical properties of BaTe, BaSe and BaS from first principles. Physica B **370**, 35–45 (2005)
22. Akhtar, M.S., Malik, M.A., Riaz, S., Naseem, S.: Room temperature ferromagnetism and half metallicity in nickel doped ZnS: experimental and DFT studies. Mater. Chem. Phys. **160**, 440–446 (2015)
23. Akhtar, M.S., Malik, M.A., Alghamdi, Y.G., Ahmad, K.S., Riaz, S., Naseem, S.: Chemical bath deposition of Fe-doped ZnS thin films: investigations of their ferromagnetic and half-metallic properties. Mater. Sci. Semicond. Proc. **39**, 283–291 (2015)
24. Tian, J.H., Song, T., Sun, X.W., Wang, T., Jiang, G.: First-principles study on the half-metallic ferromagnetism and optical properties of Fe-doped CdSe and Co-doped CdSe. Supercond. Nov. Magn. **30**, 521–528 (2017)

25. Rabbani, S.F., Banu, I.B.S.: An ab-initio calculation of half-metallic ferromagnetism in vanadium doped ZnS. J. Alloys Compd. **695**, 3131–3138 (2017)
26. Addadi, Z., Doumi, B., Mokaddem, A., Elkeurti, M., Sayede, A., Tadjer, A., Dahmane, F.: Electronic and ferromagnetic properties of 3d(V)-doped (BaS) barium sulfide. J. Supercond. Nov. Magn. **30**, 917–923 (2017)
27. Berber, M., Doumi, B., Mokaddem, A., Mogulkoc, Y., Sayede, A., Tadjer, A.: First-principle predictions of electronic properties and half-metallic ferromagnetism in vanadium-doped rock-salt SrO. J. Electron. Mater. **47**, 449–456 (2018)
28. Blaha, P., Schwarz, K., Madsen, G.K.H., Kvasnicka, D., Luitz, J.: WIEN2k, An Augmented Plane Wave Plus Local Orbitals Program for Calculating Crystal Properties. Vienna University of Technology, Vienna (2001)
29. Hohenberg, P., Kohn, W.: Inhomogeneous electron gas. Phys. Rev. **136**, B864–871 (1964)
30. Kohn, W., Sham, L.J.: Self-consistent equations including exchange and correlation effects. Phys. Rev. **140**, A1133–1138 (1965)
31. Wu, Z., Cohen, R.E.: More accurate generalized gradient approximation for solids. Phys. Rev. B **73**, 235116 (2006)
32. Tran, F., Blaha, P.: Accurate band gaps of semiconductors and insulators with a semilocal exchange-correlation potential. Phys. Rev. Lett. **102**, 226401 (2009)
33. Koller, D., Tran, F., Blaha, P.: Merits and limits of the modified Becke–Johnson exchange potential. Phys. Rev. B **83**, 195134 (2011)
34. Monkhorst, H.J., Pack, J.D.: Special points for Brillouin-zone integrations. Phys. Rev. B **13**, 5188–5192 (1976)
35. Pack, J.D., Monkhorst, H.J.: "Special points for Brillouin-zone integrations"—a reply. Phys. Rev. B **16**, 1748–1749 (1977)
36. Muranghan, F.D.: The compressibility of media under extreme pressures. Proc. Natl. Acad. Sci. U.S.A. **30**, 244–247 (1944)
37. Bhattacharjee, R., Chattopadhyaya, S.: Effects of barium (Ba) doping on structural, electronic and optical properties of binary strontium chalcogenide semiconductor compounds - A theoretical investigation using DFT based FP-LAPW approach. Mater. Chem. Phys. **199**, 295–312 (2017)
38. Chattopadhyaya, S., Bhattacharjee, R.: Theoretical study of structural, electronic and optical properties of $Ba_xPb_{1-x}S$, $Ba_xPb_{1-x}Se$ and $Ba_xPb_{1-x}Te$ ternary alloys using FP-LAPW approach. J. Alloys Compd. **694**, 1348–1364 (2017)
39. Drablia, S., Boukhris, N., Boulechfar, R., Meradji, H., Ghemid, S., Ahmed, R., Bin Omran, S., El Haj Hassan, F., Khenata, R.: Ab initio calculations of the structural, electronic, thermodynamic and thermal properties of BaSe_1 − xTe_x alloys. Phys. Scr. **92**, 105701 (2017)
40. Bahloul, B., Bentabet, A., Amirouche, L., Bouhadda, Y., Bounab, S., Deghfel, B., Fenineche, N.: Ab initio calculations of structural, electronic, optical and thermodynamic properties of alkaline earth tellurides $BaxSr_{1-x}Te$. J. Phys. Chem. Solids **75**, 307–314 (2014)
41. Grzybowski, T.A., Ruoff, A.L.: Band-overlap metallization of BaTe. Phys. Rev. Lett. **53**, 489–492 (1984)
42. Perdew, J.P., Burke, K., Ernzerhof, M.: Generalized gradient approximation made simple. Phys. Rev. Lett. **77**, 3865 (1996)
43. Goedecker, S., Teter, M., Hutter, J.: Separable dual-space Gaussian pseudopotentials. Phys. Rev. B **54**, 1703 (1996)
44. Yao, K.L., Gao, G.Y., Liu, Z.L., Zhu, L.: Half-metallic ferromagnetism of zinc-blende CrS and CrP: a first-principles pseudopotential study. Solid State Commun. **133**, 301 (2005)
45. Gao, G.Y., Yao, K.L., Şaşıoğlu, E., Sandratskii, L.M., Liu, Z.L., Jiang, J.L.: Half-metallic ferromagnetism in zinc-blende CaC, SrC, and BaC from first principles. Phys. Rev. B **75**, 174442 (2007)
46. Doumi, B., Mokaddem, A., Dahmane, F., Sayede, A., Tadjer, A.: A novel theoretical design of electronic structure and half-metallic ferromagnetism in the 3d (V)-doped rock-salts SrS, SrSe, and SrTe for spintronics. RSC Adv. **112**, 92328 (2015)
47. Cherfi, Y., Mokaddem, A., Bensaid, D., Doumi, B., Sayede, A., Dahmane, F.: A novel theoretical investigation of electronic structure and half-metallic ferromagnetism in 3d (V)-doped InP for spintronic applications. J. Supercond. Nov. Magn. **29**, 1813–1817 (2016)
48. Zolweg, R.J.: Optical absorption and photoemission of barium and strontium oxides, sulfides, selenides, and tellurides. Phys. Rev. **111**, 113–119 (1958)
49. Saum, G.A., Hensley, E.B.: Fundamental optical absorption in the IIA-VIB compounds. Phys. Rev. **113**, 1019–1022 (1959)
50. Soulen Jr., R.J., Byers, J.M., Osofsky, M.S., Nadgorny, B., Ambrose, T., Cheng, S.F., Broussard, P.R., Tanaka, C.T., Nowak, J., Moodera, J.S., Barry, A., Coey, J.M.D.: Measuring the spin polarization of a metal with a superconducting point contact. Science **282**, 85–88 (1998)
51. Zener, C.: Interaction between the d-shells in the transition metals. II. Ferromagnetic compounds of manganese with perovskite structure. Phys. Rev. **82**, 403–405 (1951)
52. Sato, K., Dederichs, P.H., Araki, K., Katayama-Yoshida, H.: Ab initio materials design and Curie temperature of GaN-based ferromagnetic semiconductors. Phys. Status Solidi C **7**, 2855–2859 (2003)
53. Sato, K., Katayama-Yoshida, H., Dederichs, P.H.: Curie temperatures of III–V diluted magnetic semiconductors calculated from first-principles in mean field approximation. J. Supercond. **16**, 31–35 (2003)
54. Akai, H.: Ferromagnetism and its stability in the diluted magnetic semiconductor (In, Mn)As. Phys. Rev. Lett. **81**, 3002–3005 (1998)